



Inter-phase charge and energy transfer in Ruddlesden–Popper 2D perovskites: critical role of the spacing cations

| | |
|-------------------------------|---|
| Journal: | <i>Journal of Materials Chemistry A</i> |
| Manuscript ID | TA-COM-02-2018-001518.R1 |
| Article Type: | Communication |
| Date Submitted by the Author: | 15-Mar-2018 |
| Complete List of Authors: | Zheng, Kaibo; Lund University, Chemical Physics Department Chen, Yani; Fudan University, Materials Science Sun, Yong; Fudan University, Materials Science Chen, Junsheng; Lunds Universitet, Chemical Physics Chabera, Pavel; Lunds Universitet, Chemical Physics Schaller, Richard; Argonne National Laboratory, Center for Nanoscale Materials Al-Marri, Mohmmmed; Qatar University, Gas Processing Center Canton, Sophie; Deutsches Elektronensynchrotron DESY, FS-ATTO Liang, Ziqi; Fudan University, Department of Materials Science Pullerits, Tonu; Lunds Universitet, Department of Chemical Physics |
| | |



Journal Name

COMMUNICATION

Inter-phase charge and energy transfer in Ruddlesden–Popper 2D perovskites: critical role of the spacing cations

Received 00th January 20xx,
Accepted 00th January 20xx

Kaibo Zheng,^{*af} Yani Chen,^b Yong Sun,^b Junsheng Chen,^a Pavel Chábera,^a Richard Schaller,^c Mohammed J. Al-Marri,^e Sophie E Canton,^{de} Ziqi Liang^{*b} and Tõnu Pullerits^{*a}

DOI: 10.1039/x0xx00000x

www.rsc.org/

Photo-generated charge carrier dynamics in Ruddlesden–Popper 2D perovskites with linear (n-BA) and branched (iso-BA) butylamine as spacing cations have been studied by using transient absorption and time-resolved photoluminescence spectroscopies. Both n-BA and iso-BA perovskites consist of mixed-phase 2D quantum wells with various layer thicknesses, where the photo-generated charges undergo inter-phase charge transfer from thinner quantum wells to thicker ones. By shortening the spacer from n-BA to iso-BA, the transfer rates are significantly increased, which can also diminish the charge accumulation in thin quantum wells induced by the unbalanced electron and hole charge transfer rates. Under high excitation intensity, the shorter spacing cation is found to further facilitate the energy transfer, which can compete with fast high-order carrier recombination and consequently improve the charge transfer efficiency. Intriguingly, we observe the existence of extra bulk 3D phases embedded within iso-BA perovskites, which can efficiently collect the confined charges within 2D phases and then transport them with faster carrier mobility and slower recombination rates.

Organometal halide perovskite materials have led the cutting-edge research on solar cells for the past several years due to their superior photophysical capabilities achieved through facile solution-processing methods.^{1–4} The record power conversion efficiency (PCE) of perovskite solar cells has now reached 22.1%, approaching the state-of-art silicon thin-film photovoltaics

(PVs).⁵ Nevertheless, the instability of the material towards ambient atmosphere, in particular moisture, remains the major bottleneck that hampers the commercialization of perovskite solar cells.⁶ The instability originates mainly from the high hydrophilicity of organic cations and the weak interaction between the organic cations and the surrounding halide anions.⁷

The emerging Ruddlesden–Popper 2D structures of halide perovskites offer a potential solution to this problem.^{8–10} In 2D perovskites, the hydrophobic long-chain organic cations — 2-phenylethylammonium (PEA) and n-butylammonium (n-BA) — partially replace the conventional methylamine cations (CH₃NH₃⁺, denoted as MA) and separate several layers of [PbI₆]^{4–} octahedra to form quantum well domains.¹¹ Those hydrophobic spacing cations could effectively prevent the penetration of ambient water molecules, thereby greatly enhancing air stability.¹² However, due to the disconnected inorganic semiconducting network in the direction of the spacing cations in the Ruddlesden–Popper structure, the charge carrier transport is drastically limited, decreasing the photocurrent in PV devices.⁸ Recent studies have introduced the so-called ‘hot-casting’ fabrication method to orient 2D perovskites preferentially in the out-of-plane direction, where the 2D planes can efficiently connect the electron and hole selective electrode layers with improved charge carrier transport and device performance.¹³ Alternatively, the internal charge transfer or energy transfer between the quantum wells mediated by the long-chain spacing cations have also been identified in 2D perovskites.^{14–16} Since such transfer processes strongly depend on the electronic coupling between the neighboring quantum wells, tailoring the spacing cations could be another powerful approach to improve charge transport in 2D perovskites. Our recent work has indicated that replacing the linear n-BA spacing cation with the shorter branched iso-butylammonium (namely, iso-BA) in 2D perovskites can significantly improve the PV performance of the device.¹⁷ Time-resolved THz spectroscopy investigation also revealed the increased out-of-plane charge carrier mobilities in iso-BA

^aDepartment of Chemical Physics and NanoLund, Lund University, Box 124, 22100, Lund, Sweden. *Email: kaibo.zheng@chemphys.lu.se, tonu.Pullerits@chemphys.lu.se

^bDepartment of Materials Science, Fudan University, Shanghai 200433, China. *Email: zqliang@fudan.edu.cn

^cCenter for Nanoscale Materials, Argonne National Laboratory, 9700 Cass Avenue, Argonne, Illinois 60439, United States

^dELI-ALPS, ELI-HU Non-Profit Ltd., Dugonicster 13, Szeged 6720, Hungary

^eAttoscience Group, Deutsche Elektronen Synchrotron (DESY), Notkestrasse 85, D-22607 Hamburg, Germany

^fGas Processing Center, College of Engineering, Qatar University, PO Box 2713, Doha, Qatar

†Electronic Supplementary Information (ESI) available: [Experimental details, TA kinetics, Luminescence quantum yield]. See DOI: 10.1039/x0xx00000x

perovskite films compared to the n-BA counterparts. However, the detailed charge carrier dynamics and the corresponding structural correlation still remain to be understood.

In this work, we conduct a detailed investigation on the photo-generated charge carrier dynamics in n-BA and iso-BA 2D perovskites by using transient absorption and time-resolved photoluminescence spectroscopies. Our results demonstrate that the charge transfer among 2D quantum wells in iso-BA perovskites with a shorter spacing cation is twice faster than in n-BA perovskites. In addition, the charge migration for electrons and holes is more balanced in iso-BA perovskites preventing possible charge accumulation. The 3D phases existing in room-temperature processed iso-BA perovskites also serve as charge reservoirs to further improve the efficiency of charge carrier transportation. At high excitation intensity, we also observed fast energy transfer in iso-BA perovskites. This transfer can compete with the multi-exciton recombination processes, which may accelerate the applications in LED or lasing devices.

In the 2D perovskite quantum wells, $[\text{PbI}_6]^{4-}$ octahedra are separated by two layers of the organic moiety. In our work, we selected two spacing cations: conventional linear (n-BA) and branched (iso-BA) butylamine spacers as shown in Fig. 1a. Both samples have pronounced peaks at 14.10° and 28.37° in the X-ray diffraction (XRD) patterns attributed respectively to the characteristic (111) and (202) lattice planes of Ruddlesden-Popper 2D perovskites.¹⁸ The existence of pronounced and narrowed diffraction peaks in iso-BA perovskite compared to n-BA perovskite suggests better crystallinity and larger grain sizes. In addition, the dominant (202) peaks in iso-BA perovskites indicate the possible out-of-plane preferential orientation on the substrate, which has been systematically discussed in our previous work.¹⁷ Owing to quantum confinement, the mono-phase 2D perovskites exhibit the signature exciton bands in their absorption spectra, which are red-shifted as the thickness of the quantum wells (i.e., numbers of octahedral layers n in $(\text{BA})_n(\text{CH}_3\text{NH}_3)_{n-1}\text{Pb}_n\text{I}_{3n+1}$) is increased.

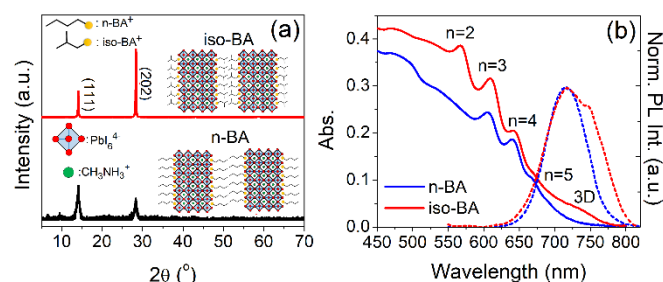


Fig. 1 (a) XRD patterns of n-BA and iso-BA perovskite film with corresponding chemical and crystal structures. (b) UV-vis absorption (solid lines) and PL (dashed lines) spectra of as-obtained n-BA and iso-BA perovskite films, in which the characteristic exciton bands for 2D quantum wells with different thicknesses are indicated.

However, in relatively thick perovskite films (~ 280 nm, as shown in Fig. S1 in Electronic Supplementary Information, ESI[†]) which have been widely employed in PV devices, some extent of mixed 2D phases with various n values cannot be avoided due to the synthetic process. This can be easily evidenced in the

absorption spectra as shown in Fig. 1b where the characteristic exciton peaks for $n = 2$ to 5 at 568, 609, 644 and 670 nm can be observed in n-BA perovskites.¹⁴ The exciton bands from $n = 3$ to 5 phases can also be resolved in iso-BA samples. We point out an extra non-negligible absorption band at 740 nm in iso-BA perovskite, which is similar to the band-edge absorption of bulk 3D perovskites. This indicates a substantial 3D phase embedded within 2D structures in iso-BA perovskites. Consequently, the photoluminescence (PL) spectrum of iso-BA perovskite also exhibits notable red shift relative to that of n-BA perovskites (see Fig. 1b) which does not have any red-shifted 3D band. The iso-BA emission clearly consists of two bands with the first one at 710 nm and the second at 750 nm. The emission spectrum of n-BA perovskite only shows a single band at 710 nm, which is most likely mainly contributed by the band-edge radiative recombination of charge carriers in 2D phases. In iso-BA perovskites both 2D and 3D phases emit photons upon light excitation. The following investigation on the detailed excited state dynamics confirms this argumentation. It should be noted that using hot-casting synthesis method, also n-BA 2D perovskite can contain 3D phase, which will greatly influence the charge carrier dynamics.¹⁴ Here, we demonstrate that under conventional RT preparation conditions, substantial 3D phases are induced in iso-BA perovskite, rather than in n-BA analogues, which can be an advantage for charge transportation as will be explained in the following part.

In order to interrogate the charge carrier transport within the 2D perovskite films, we conducted transient absorption (TA) measurements. The standard solar radiation (AM 1.5G) yields an excitation density between 10^{13} to 10^{15} cm^{-3} for conventional 3D lead halide perovskite films.¹⁹ In order to resemble the PV excitation regime, we first excited our samples at a low intensity of the laser pulse (3×10^{12} ph/cm²/pulse) which corresponds to an excitation density of $\sim 3 \times 10^{16}$ cm^{-3} (for calculation details in the SI). Fig. 2a,b show that the TA spectrograms of both samples consist of negative (blue) ground state bleach together with stimulated emission and positive (red) excited state absorption. Clear bleach bands appear in TA spectra at the wavelengths where the exciton peaks of the various n -number structures absorb. In the n-BA perovskite sample only the bleach of the 2D phase excitation (i.e., 602 nm for $n = 3$, 645 nm for $n = 4$, and 670 nm for $n = 5$) can be observed with negligible 3D phase bleach at 740 nm, while in iso-BA perovskite, the bleach of the 3D phase at 740 nm is pronounced.

The time evolution of the bleach features with concomitant decay and rise components with similar timescales provides clear evidence of excitation redistribution due to charge transfer or energy transfer among the various phases of the thin film.¹⁴ We also point out that the TA dynamics does not show any significant spatial difference as illustrated in Fig. S2. We conclude that the various 2D phases form a homogeneously mixed film at tens of μm scale. The singular value decomposition (SVD) fitting of the TA spectra was performed to extract the spectral components representing the different timescales of the charge carrier dynamics, as shown in Fig. 2c,d. The TA spectra of n-BA perovskite can be fitted by a fast (0.3 ± 0.1 ps), an intermediate (350 ± 2 ps) and a slow (19 ± 1 ns) component. The slow component is attributed to the monomolecular recombination of the photo-generated electrons and holes at $n = 3, 4, 5$ phases as the bleaching induced by the state filling at each phase can be well recognized. The fast component with 0.3 ps lifetime only exhibits a bleach band for $n = 3$ and 4 with the position slightly blue shifted in comparison with the slow

component. The sub-picosecond lifetime and the blue-shift of the bleach are the typical features of thermalization and dissociation of excitons.²⁰ The positive bands of the fast component at 580 nm, 610 nm and 670–750 nm can be ascribed to the excited state absorption (ESA) to doubly excited state as highlighted by dashed circles in Fig. 2a. According to the previous report, the exciton binding energy for n-BA 2D perovskites ranges from 150–200 meV with n values from 3 to 5.¹⁵ According to the Saha-Langmuir equation, this means that at low excitation intensity 60% of initial photo-generated species are free charges (the details of free charge vs. exciton calculation are shown in the SI).¹⁷ The efficient exciton dissociation (< 1 ps) that is attributed to the special edge states in 2D perovskites further guarantees that the majority of the photo-generated species visible in the spectroscopies under these conditions are free carriers.¹⁵ This can be further confirmed by the featureless positive absorption at the IR region as shown in Fig. S3.

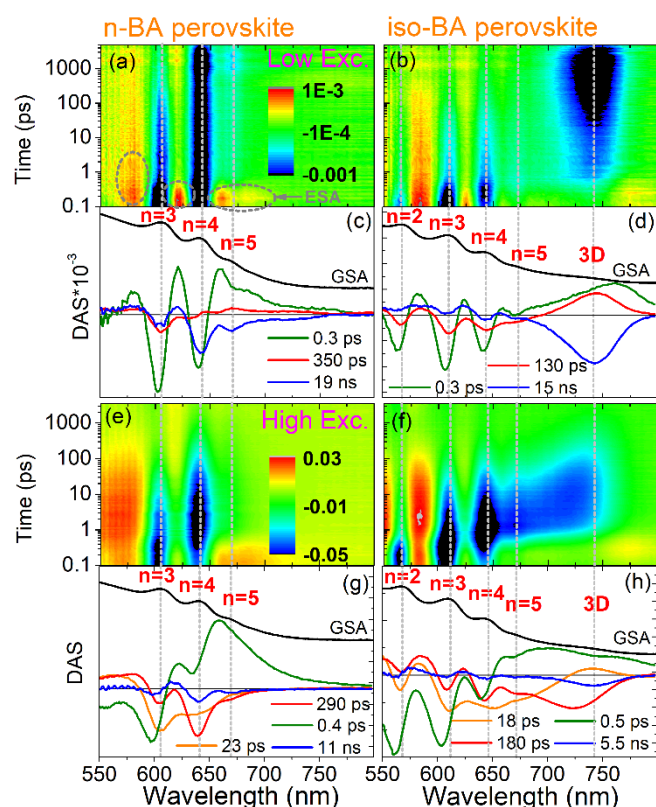


Fig. 2 TA spectra of (a) n-BA and (b) iso-BA perovskites, respectively, with 400 nm excitation at a laser fluence of 3×10^{12} ph/cm²/pulse. (c) and (d) are the SVD fitted spectral components of the corresponding TA spectra. TA spectra of (e) n-BA and (f) iso-BA perovskites, respectively, with 400 nm excitation at a laser fluence of 1.5×10^{14} ph/cm²/pulse. (g) and (h) are the SVD fitted spectral components of the corresponding TA spectra.

The intermediate 350 ps component shows concurrently negative signal at the bleach position of the $n = 3$ phase and positive signals of the $n = 4, 5$ and 3D phases. Unlike in fast component, the positive bands in the intermediate component should be attributed to the rising of the bleach as confirmed by the TA kinetics at the corresponding wavelength in Fig. S4. This is an evidence of a simultaneous depopulation of excited states in the $n = 3$ phase and a population of excited states in the other two phases (i.e., $n = 4$ and 5) associated to a charge transfer or energy transfer in-between

phases. In order to distinguish these two processes, time-resolved photoluminescence (TRPL) measurements were carried out on both samples with similar excitation conditions as shown in Fig. 3a, b. The SVD fitting of the PL spectra in n-BA perovskite (Fig. 3c) shows a slow component of 15 ± 1 ns representing the excited state lifetime. Carrier recombination involves both radiative and nonradiative pathways. Under the same excitation conditions as the time-resolved measurement, the absolute PL quantum yield (PLQY) is 60% (for details see Fig. S5). Since the excited state lifetime τ_{long} in TRPL represents the sum of radiative recombination and nonradiative trapping, we can determine the nonradiative trapping time τ_{T} and purely radiative lifetime τ_{rad} from PLQY as follows:

$$\text{PLQY} = \tau_{\text{long}} / \tau_{\text{rad}} \quad (1)$$

$$1/\tau_{\text{long}} = 1/\tau_{\text{rad}} + 1/\tau_{\text{T}} \quad (2)$$

giving rise to,

$$\tau_{\text{T}} = \tau_{\text{long}} / (1 - \text{PLQY}) \quad (3)$$

We thus obtain the τ_{T} for n-BA and iso-BA perovskites as 37 and 40 ns, respectively, while τ_{rad} for n-BA and iso-BA perovskites are 25 and 17 ns, respectively. Such slow nonradiative charge recombination is most likely due to the trapping followed by long-distance charge carrier diffusion.

The fast PL component (2.7 ± 0.1 ns) consists of the positive and negative contributions on the blue and red sides, respectively, which corresponds to the charge or energy transfer among phases. We can first exclude the energy transfer since in this case the component should also appear in the TA spectra. Given that the hole states are more closely spaced compared to the electron states in 2D perovskites according to the DFT calculations, the signal of the TA bleaching is dominated by the state filling of rather electrons than holes.¹¹ This was previously verified in other quantum confined systems such as colloidal quantum dots.²¹ Therefore, we assign the 2.7 ns component in TRPL to hole transfer ($\tau_{\text{HT-nBA}} = 2.7$ ns). On the other hand, the apparatus response function in the streak camera experiment (~ 500 ps) does not allow to resolve the 350 ps component observed in TA. The component can originate from either inter-phase energy transfer or electron transfer. If the 350 ps energy transfer would occur simultaneously with the 2.7 ns hole transfer, we would not be able to observe the slower process since it would be shortcut by the significantly faster energy transfer. An alternative scenario could be that the energy transfer and the hole transfer are independent of each other since they would occur at different locations. However, this would mean spatial non-uniformity of the dynamics which contradicts the results from the spatially resolved TA measurements that demonstrate homogeneity (for details see Fig. S2). Hence, we conclude that the 350 ps component is the inter-phase electron transfer. Such different transfer speeds for electrons and holes is consistent with the previous observations.¹⁴

Next, we verify that the time-scale of the charge transfer is mainly associated to the interfacial charge injection instead of prior exciton migration to the interface. Such exciton diffusion has been observed in both 3D and 2D perovskite systems.¹⁶ Here we also prepared the n-BA perovskite sample with the hot-casting method which was reported to induce reorientation of the 2D quantum wells on the substrate.¹³ The TA data show that the inter-phase charge transfer time (310 ps) is similar to that of the conventional RT prepared samples regardless of the morphological deviation (for details see Fig. S6). This means that the inter-phase charge transfer in n-BA perovskite is determined by the inter-phase spacing cations, which is the only common parameter between these two cases.

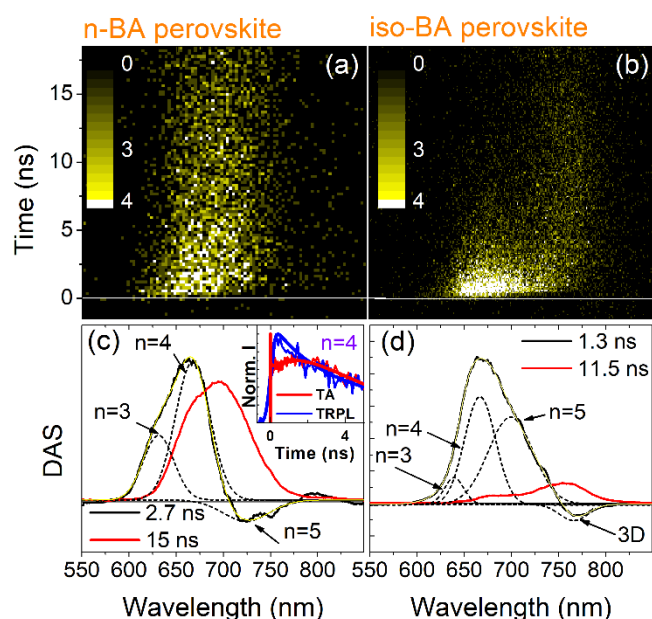


Fig. 3 TRPL spectra of (a) n-BA perovskite and (b) iso-BA perovskite with 400 nm excitation at a laser fluence of 3×10^{12} ph/cm²/pulse. (c) and (d) are the SVD fitted spectral components of the corresponding TRPL spectra. The dashed black line represents the Gaussian peak fitting of the convoluted spectra curve showing contribution from various n phases.

Based on the above analysis, the inter-phase charge transfer can be tuned if the spacing cation is changed. Here we replaced the linear n-BA with shorter non-linear iso-BA chains. In this case the main bleach component in TA resides in the 3D phases as shown in Fig. 2b. The SVD fitting of the spectra yields three components (Fig. 2d). As shown by the fast component, the mixed 2D phase from the $n = 2$ to 5 in iso-BA perovskite all absorb at the excitation wavelength. However, the final slow component exhibits the dominant bleach in the 3D phase, implying that most of the charges in the 2D phase have been transferred to the 3D phase. The intermediate component indicates that the electron transfer time in this case is 2 times faster than in n-BA perovskite ($\tau_{\text{ET-iso-BA}} = 130.0 \pm 2.0$ ps). Accordingly, the hole transfer time ($\tau_{\text{HT-iso-BA}} = 1.3 \pm 0.1$ ns) in iso-BA perovskite is also twice shorter than that of n-BA perovskite (2.7 ± 0.1 ns) as extracted from the TRPL in Fig. 3d. The difference in charge transfer rate between the two samples for both electron and hole transfer can be qualitatively explained by the tunnelling barrier induced by the spacing cations. The shortening of the spacing cations by using iso-BA (~ 10 Å) compared with n-BA (~ 13 Å)¹¹ would narrow the barrier. For more quantitative description, however, an analysis of the orbital topology of the linking ligand molecules would be needed.²²

An interesting observation is that the TA spectra and the SVD fitting of n-BA perovskite in Fig. 2a,c indicate that the electron transfer occurs from $n = 3$ phase to $n = 4, 5$ and 3D phases, while TRPL spectra in Fig. 3a,d suggest that the hole transfer occur from the $n = 3, 4$ phase to the $n = 5$ phase. The simultaneous population of electrons and depopulation of holes at $n = 4$ phase can be clearly observed in the comparison of TA and TRPL kinetics as shown in the inset of Fig. 3c. Such unbalanced charge transfer induces electron

accumulation at the $n = 4$ phase in n-BA perovskite film. This could prevent efficient charge transport to the respective electrodes and thereby reduce the short-circuit current of the solar cell device, which has been observed in our previous work.¹⁷ On the other hand, in iso-perovskite both electrons and holes are swiftly transferred to the final 3D phase with negligible residual electrons in the 2D phases as evidenced by the line shape of TA component after charge transfer (see the blue line in Fig. 2d). Accordingly, the prototype solar cell based on iso-BA perovskites exhibited a short-circuit current density (J_{sc}) 2 times higher than that of an n-BA perovskites based device.¹⁷

When the excitation intensity is much higher than in the PV regime with photon density $n_0 > 10^{16}$ cm⁻³, the difference of the inter-phase charge transfer between the two samples becomes more pronounced. Fig. 2e,f show the TA spectra of n-BA and iso-BA perovskites with an excitation photon density of 1.5×10^{18} cm⁻³. We point out that at such a high excitation density more than 95% of the photo-generated species after the equilibration are excitons (the details of calculation are shown in the SI). In this regard, higher order recombination dynamics can occur in addition to the conventional transport and first-order monomolecular recombination of photo-generated excitons in the 2D phases. The SVD of the TA dynamics in n-BA perovskite provides 4 time-components. The fastest component (0.4 ± 0.1 ps) and slowest component (11 ± 1 ns) resemble the spectral state-filling features and lifetimes of the low excitation condition and have the similar origin – fast cooling of the initial state and slow recombination of the final state. We notice that the single exciton recombination is slightly faster than the monomolecular recombination of free charges at low excitation intensity (19 ns). Apart from that, we can extract two components both showing negative bleaching from the $n = 3, 4, 5$ phases with lifetimes of 290 ± 2 and 23 ± 1 ps, respectively. Alternatively, the first 30 ps TA signal can be well described via a clear linear relationship between the second order inverted differential absorption signal ΔA^{-2} and time (see Fig. S7). This strongly suggests that the third order recombination contributes to the early dynamics:²³

$$-\frac{dN(t)}{dt} = CN^3, \quad (4)$$

where N refers to the photo-generated carrier concentration which is proportional to the differential absorption (ΔA) in the TA spectra. Considering that we mainly have excitons as photo-generated species, the fast excited-state decay dynamics within tens to hundreds of ps is dominated by Auger recombination. No typical feature of charge transfer can be identified as almost no positive signal opposite to the bleach band can be found since the nonlinear electron-hole recombination is much faster than the inter-phase charge transfer under multi-exciton condition.

In iso-BA perovskite, however, we observe one component with a lifetime of 18 ± 2 ps showing both positive and negative signals at the bleach positions, see Fig. 2h (black line). The relatively poor linear fit to the ΔA^{-2} and ΔA^{-1} vs time plots indicates that this component should not be assigned to the high order recombination process as shown in Fig. S8. It cannot be due to the hot charge transfer either since the negative part of the signal does not show any blue shift compared to the single exciton band (bleach at the olive curve). Instead, it most likely corresponds to a fast excited state transfer process from 2D phases to 3D phases which can compete with the high order recombination process. This is apparently facilitated by

the shorter spacing between the phases but the detailed transfer dynamics can be complicated. In our previous work, we found that at high excitation intensity the excited charges for perovskite nanoparticles would undergo accumulation towards high energy level which can cross the energy barrier and be trapped by the surface traps. Such charge accumulation could also facilitate the inter-phase charge transfer. Furthermore, an enhanced energy transfer was found from multi-excitons in single quantum dot to dye molecule compared to single exciton condition due to the larger transition dipole from the bi-exciton to single exciton.²⁴ We point out, however, that in absorption an opposite trend has been found—the transition from single to bi-exciton state is weaker than the ground to a single-exciton state.^{25,26} Still, the 18 ps component here can be due to the energy transfer from the 2D to the 3D phase via multi-exciton transitions in the donor.

One could obtain a clearer picture regarding different charge carrier dynamics for n-BA and iso-BA perovskites at high excitation intensity by reviewing the detailed measurements of excitation intensity dependence as shown in Fig. S9. In n-BA sample, the inter-phase charge transfer can be observed only at the lowest excitation intensity while in iso-BA such excited state population transfer always exists even at the higher excitation intensities. This clearly confirms our argument that in iso-BA sample, the inter-phase charge transfer will not be surpassed by the fast Auger charge recombination.

Fig. 4 summarizes the inter-phase charge/energy transfer in these two types of 2D perovskite structures under both low- and high-intensity excitation regimes. Here the observed charge transfer dynamics—both electrons and holes are transferred down-stream from 2D phases to 3D phases—indicates that the energy band alignment should be type-I rather than type-II as measured by the ultraviolet photoelectron spectroscopy (UPS) reported in the literature.¹⁸ This should be attributed to the deviation between volume states and low energy edge states at the interface of the quantum wells within 2D perovskites.¹⁵ Thus we can conclude: 1) The enhanced inter-phase electronic coupling in case of shorter iso-BA ligand accelerates the down-streaming of the photo-generated charges from the quantum confined domains to less confined bulk phases. 2) The 3D phases that exist in iso-BA perovskites would efficiently collect the confined charges within 2D phases and transport them with faster carrier mobility and slower recombination rates. In contrast, such 3D phases are only found in n-BA perovskites when employing the hot-casting method, which is not necessarily required in iso-BA perovskites. 3) The efficient inter-phase charge transfer effectively reduces the charge accumulation at a certain phase caused by the unbalanced transfer of electrons and holes due to the different band alignment between the conduction and valence bands in 2D perovskites. We propose that these three factors are the main photo-physical origins for the better performance of iso-BA perovskite solar cells than the n-BA counterparts besides the favourable orientation of the 2D perovskite plates in the former.¹⁷ At high excitation intensity which reflect the situation in LED or lasing devices, excitons dominate the photo-induced species. The shortening of the spacing cations is more critical since the required charge separation or energy migration need to compete with the multi-exciton recombination. In this scenario, directed energy

transfer in iso-BA perovskite is still feasible, which is not surpassed by faster high-order Auger recombination processes.

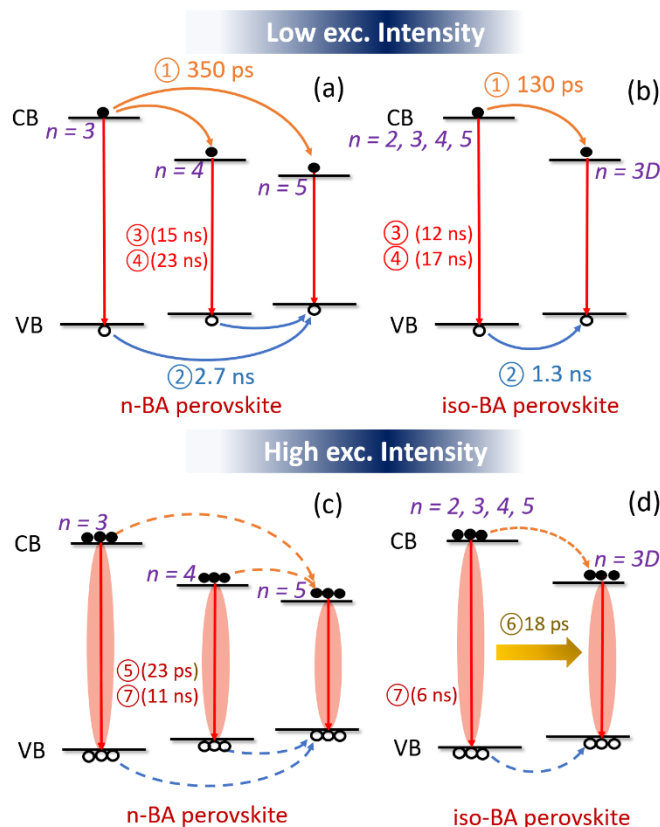


Fig. 4 Schematics of the dominating channels of the excited state depopulation ① electron transfer, ② hole transfer, ③ monomolecular radiative recombination, ④ monomolecular non-radiative recombination, ⑤ Auger recombination, ⑥ energy transfer and ⑦ single exciton recombination; for (a) n-BA perovskite and (b) iso-BA perovskite under (a, b) low and (c, d) high excitation intensity, respectively. The dashed lines in (c) and (d) indicate decreased contribution of the electron (filled circle) and hole (open circle) transfer, respectively.

In conclusion, we have investigated the photo-induced charge carrier dynamics in two types of Ruddlesden–Popper 2D perovskites films with linear and branched spacing cations, respectively, using both TA and TRPL spectroscopy methods. The inter-phase charge/energy transfer is greatly accelerated by shorter spacing cations, which prevents the charge accumulation resulting from the unbalanced transfer rates between electrons and holes. In addition, the shorter spacing cation ensures the efficient exciton migration from 2D to 3D phases even under high-intensity light excitation without high-order charge recombination. Moreover, the existence of the 3D bulk phases observed in 2D perovskites with a shorter spacing cation can serve as charge reservoirs to inhibit excitonic recombination and such 3D/2D mixed phases can be easily achieved in room-temperature processed iso-BA perovskites. We anticipate that these findings will guide the development of microscopic molecular design for Ruddlesden–Popper 2D perovskites in the future device applications.

Conflicts of interest

There are no conflicts to declare.

Acknowledgements

This work was made possible by NPRP grant #7-227-1-034 from the Qatar National Research Fund (a member of Qatar Foundation). Z.L. thanks the support from Inter-Governmental International Cooperation Projects of Science and Technology Commission of Shanghai Municipality (STCSM) under grant No. 17520710100. We also acknowledge financial support by the Swedish Research Council, KAW foundation, Swedish Energy Agency and STINT. Use of the Center for Nanoscale Materials, an Office of Science user facility, was supported by the U.S. Department of Energy, Office of Science, Office of Basic Energy Sciences, under Contract No. DE-AC02-06CH11357. The ELI-ALPS project (GINOP-2.3.6-15-2015-00001) is supported by the European Union and co-financed by the European Regional Development Fund.

Notes and references

- 1 H.-S. Kim, C.-R. Lee, J.-H. Im, K.-B. Lee, T. Moehl, A. Marchioro, S.-J. Moon, R. Humphry-Baker, J.-H. Yum, J. E. Moser, M. Grätzel and N.-G. Park, *Sci. Rep.*, 2012, **2**, 591.
- 2 M. M. Lee, J. Teuscher, T. Miyasaka, T. N. Murakami and H. J. Snaith, *Science*, 2012, **338**, 643–647.
- 3 N. J. Jeon, J. H. Noh, W. S. Yang, Y. C. Kim, S. Ryu, J. Seo and S. I. Seok, *Nature*, 2015, **517**, 476–480.
- 4 J. Peng, Y. Chen, K. Zheng, T. Pullerits and Z. Liang, *Chem. Soc. Rev.*, 2017, **46**, 5714–5729.
- 5 W. S. Yang, B.-W. Park, E. H. Jung, N. J. Jeon, Y. C. Kim, D. U. Lee, S. S. Shin, J. Seo, E. K. Kim, J. H. Noh and S. I. Seok, *Science*, 2017, **356**, 1376–1379.
- 6 J. S. Manser, M. I. Saidaminov, J. A. Christians, O. M. Bakr and P. V. Kamat, *Acc. Chem. Res.*, 2016, **49**, 330–338.
- 7 J.-W. Lee, D.-H. Kim, H.-S. Kim, S.-W. Seo, S. M. Cho and N.-G. Park, *Adv. Energy Mater.*, 2015, **5**, 1501310.
- 8 Y. Chen, Y. Sun, J. Peng, J. Tang, K. Zheng and Z. Liang, *Adv. Mater.*, 2018, **30**, 1703487.
- 9 T. Zhang, L. Xie, L. Chen, N. Guo, G. Li, Z. Tian, B. Mao and Y. Zhao, *Adv. Funct. Mater.*, 2017, **27**, 1603568.
- 10 T. Zhang, M. I. Dar, G. Li, F. Xu, N. Guo, M. Grätzel and Y. Zhao, *Sci. Adv.*, 2017, **3**, e1700841.
- 11 C. C. Stoumpos, D. H. Cao, D. J. Clark, J. Young, J. M. Rondinelli, J. I. Jang, J. T. Hupp and M. G. Kanatzidis, *Chem. Mater.*, 2016, **28**, 2852–2867.
- 12 B. Li, C. Fei, K. Zheng, X. Qu, T. Pullerits, G. Cao and J. Tian, *J. Mater. Chem. A*, 2016, **4**, 17018–17024.
- 13 H. Tsai, W. Nie, J.-C. Blancon, C. C. Stoumpos, R. Asadpour, B. Harutyunyan, A. J. Neukirch, R. Verduzco, J. J. Crochet, S. Tretiak, L. Pedesseau, J. Even, M. A. Alam, G. Gupta, J. Lou, P. M. Ajayan, M. J. Bedzyk, M. G. Kanatzidis and A. D. Mohite, *Nature*, 2016, **536**, 312–316.
- 14 J. Liu, J. Leng, K. Wu, J. Zhang and S. Jin, *J. Am. Chem. Soc.*, 2017, **139**, 1432–1435.
- 15 J.-C. Blancon, H. Tsai, W. Nie, C. C. Stoumpos, L. Pedesseau, C. Katan, M. Kepenekian, C. M. M. Soe, K. Appavoo, M. Y. Sfeir, S. Tretiak, P. M. Ajayan, M. G. Kanatzidis, J. Even, J. J. Crochet and A. D. Mohite, *Science*, 2017, **355**, 1288–1292.
- 16 G. Xing, B. Wu, X. Wu, M. Li, B. Du, Q. Wei, J. Guo, E. K. L. Yeow, T. C. Sum and W. Huang, *Nat. Commun.*, 2017, **8**, 14558.
- 17 Y. Chen, Y. Sun, J. Peng, W. Zhang, X. Su, K. Zheng, T. Pullerits and Z. Liang, *Adv. Energy Mater.*, 2017, **7**, 1700162.
- 18 D. H. Cao, C. C. Stoumpos, O. K. Farha, J. T. Hupp and M. G. Kanatzidis, *J. Am. Chem. Soc.*, 2015, **137**, 7843–7850.
- 19 V. D'Innocenzo, G. Grancini, M. J. Alcocer, A. R. Kandada, S. D. Stranks, M. M. Lee, G. Lanzani, H. J. Snaith and A. Petrozza, *Nat. Commun.*, 2014, **5**, 3586.
- 20 M. B. Price, J. Butkus, T. C. Jellicoe, A. Sadhanala, A. Briane, J. E. Halpert, K. Broch, J. M. Hodgkiss, R. H. Friend and F. Deschler, *Nat. Commun.*, 2015, **6**, 8420.
- 21 K. Zheng, K. Židek, M. Abdellah, W. Zhang, P. Chábera, N. Lenngren, A. Yartsev, T.T. Pullerits, P. Chabera, N. Lenngren, A. Yartsev and T. Pullerits, *J. Phys. Chem. C*, 2014, **118**, 18462–18471.
- 22 T. Hansen, K. Židek, K. Zheng, M. Abdellah, P. Chábera, P. Persson and T. Pullerits, *J. Phys. Chem. Lett.*, 2014, **5**, 1157–1162.
- 23 J. S. Manser and P. V. Kamat, *Nat. Photon.*, 2014, **8**, 737–743.
- 24 X. Huang, Q. Xu, C. Zhang, X. Wang and M. Xiao, *Nano Lett.*, 2016, **16**, 2492–2496.
- 25 K. Zheng, K. Židek, M. Abdellah, N. Zhu, P. Chábera, N. Lenngren, Q. Chi and T. Pullerits, *J. Am. Chem. Soc.*, 2014, **136**, 6259–6268.
- 26 N. Lenngren, T. Gating, K. Zheng, M. Abdellah, N. Lascoux, F. Ma, A. Yartsev, K. Židek and T. Pullerits, *J. Phys. Chem. Lett.*, 2013, **4**, 3330–3336.